



Lasers in Manufacturing Conference 2023

Enhancement of additive manufactured soft magnetic components by precise air gaps combining laser powder bed fusion and ultrafast laser ablation

David Kolb^{a,*}, Markus Hofele^a, Manuel Henn^b, Matthias Buser^b, Volkher Onuseit^b,
Thomas Graf^b, Harald Riegel^a

^aLaserApplicationCenter (LAZ), Aalen University, Beethovenstraße 1, 73430 Aalen, Germany

^bInstitut für Strahlwerkzeuge (IFSW), University of Stuttgart, Pfaffenwaldring 43, 70569 Stuttgart, Germany

Abstract

Laser Powder Bed Fusion (PBF-LB) additive manufacturing offers great potential for the production of efficiency- and performance-enhancing soft magnetic materials and components for electrical machines. One way to reduce remagnetization losses in soft magnets is to inhibit the propagation of eddy currents through geometric design. This results in the need for very fine eddy current inhibiting insulating air gaps. However, PBF-LB is limited in terms of achievable accuracy and minimum size of electrically separated structures $>100\ \mu\text{m}$ due to the inherent micro-melting process. In this work, the PBF-LB process is combined with layer-wise ultrafast laser ablation to create precise air gaps in the range of $25\text{-}45\ \mu\text{m}$ in soft magnets made of pure iron. Magnetic characterization revealed a reduction of iron losses in the alternating magnetic field with frequencies of $25\text{-}200\ \text{Hz}$ of up to 44% in the as-built condition and up to 39% in the heat-treated condition.

Keywords: Selective laser melting; Ultrashort pulsed laser; Magnets; Laser ablation; Internal structures; Combined machining

1. Introduction

Laser Powder Bed Fusion (PBF-LB) additive manufacturing offers great potential for the production of efficiency- and performance-enhancing soft magnetic materials and components for next-generation electric

* Corresponding author. Tel.: +49 7361 576 2669.
E-mail address: david.kolb@hs-aalen.de.

machine (EM) designs. In this context, the PBF-LB process enables completely novel soft magnetic component architectures with, for example, three-dimensional magnetic flux or heat dissipation paths that can be specifically tailored to the EM design (Lamichhane et al., 2020; Pham et al., 2021; Giannotta et al., 2023). In addition, PBF-LB enables the processing of performance-enhancing soft magnetic materials, such as iron with a high silicon content of 6.5 wt.%, where conventional manufacturing processes reach their limits, as well as the targeted adjustment of grain size and grain orientation (Garibaldi et al., 2018; Plotkowski et al., 2019; Goll et al., 2019; Goodall et al., 2023). However, effective fabrication strategies still need to be developed to efficiently limit remagnetization losses in PBF-LB soft magnetic bulk components in order to fully exploit the potential of additive manufacturing. In addition to adjusting the material composition and introducing insulating layers, it has been shown that separating the soft magnetic core volume by air gaps or finite internal material structures have a positive effect on reducing eddy current losses (Goll et al., 2019; Plotkowski et al., 2019; Tiismus et al., 2021; Kresse et al., 2022; Goodall et al., 2023). However, the introduction of air gaps reduces the fill factor by reducing the volume of the soft magnetic material and thus the magnetic power density, which in turn would have to be compensated, e.g., by increasing the volume of the machine. In this context, there is a need to create the smallest possible air gap eddy current confinement structures. However, due to the inherent micro-melting process, PBF-LB is limited in the achievable surface accuracy of the structure walls to a minimum distance of the electrically separated structures (air gap width) of $>100\ \mu\text{m}$ (Kresse et al., 2022; Goodall et al., 2023). In order to overcome the limitations of the PBF-LB process and to fabricate smaller air gaps in soft magnetic components, a quasi-simultaneous laser fabrication process consisting of PBF-LB and layer-wise ultrafast laser ablation is used in this work and the influence of the air gaps on the magnetic properties is analyzed. With this laser process combination, air gaps with a width of less than $50\ \mu\text{m}$ have already been achieved in PBF-LB fabricated parts (Henn et al., 2021; Henn et al., 2022).

2. Experimental setup and methodology

2.1. Experimental setup

A quasi-simultaneous manufacturing process combining additive and subtractive laser processes was used for the experimental investigations. Fig. 1 shows a schematic representation of the combined laser manufacturing process. A thin-disk continuous wave laser (CW laser) is used for the additive PBF-LB process and an ultrafast laser (USP laser) is used for the subtractive material ablation to create the air gaps. Both laser sources emit at a wavelength of 1030 nm, are guided in the same beam path and are coupled into a common focusing optic. A galvanometer 2D scanner with a f-theta lens and a focal length of 163 mm was used as focusing optic. The focal diameter of the CW laser is about $200\ \mu\text{m}$ and that of the USP laser is about $35\ \mu\text{m}$. Switching between the laser sources was done by a flip mirror. A homemade modular powder bed process chamber equipped with various sensors was used for the manufacturing of the soft magnetic components. The process chamber consists of a closed, inert gas-fillable build space (maximum component dimensions $\varnothing = 100\ \text{mm}$, height 100 mm) with a glass entrance window transparent for the two laser beams used and an associated gas circulation and purification system. Experiments were performed without preheating the substrate plate of the powder bed process chamber. All components are integrated into a flexible multi-axis laser processing station and are fully automatically controlled by a CNC / PC unit.

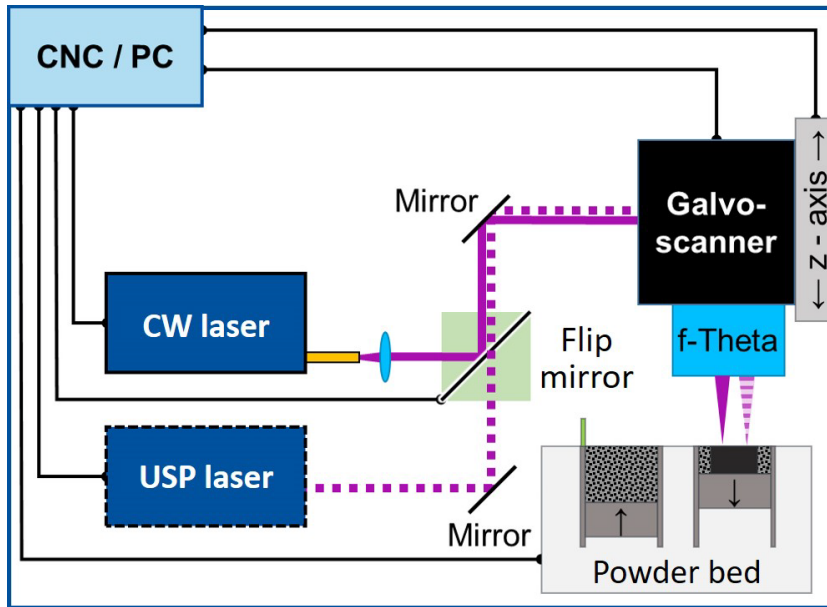


Fig. 1. Schematic representation of the combined additive and subtractive laser manufacturing process

2.2. Material

For the experiments, gas-atomized pure iron powder is utilized. The powder material is composed of predominantly spherical particles with an average particle size D_{50} of approximately $35\ \mu\text{m}$, while D_{10} and D_{90} are $20\ \mu\text{m}$ and $50\ \mu\text{m}$, respectively. Particle size distribution and a scanning electron image of the iron powder are shown in Fig. 2.

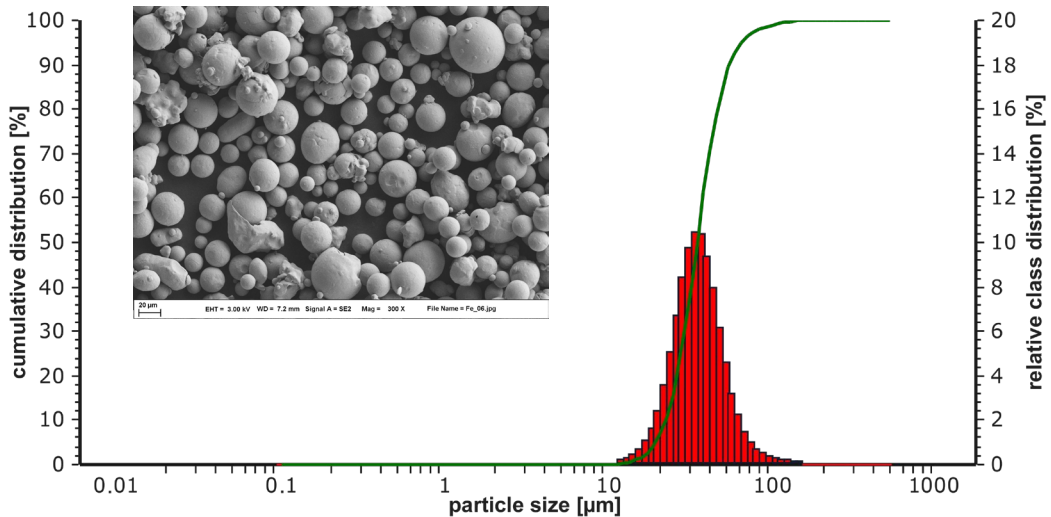


Fig. 2. Particle size distribution and scanning electron image of the iron powder: the green curve shows the cumulative particle size distribution ranging from 0% to 100%. The red bars present the relative percentage of the particle size classes

2.3. Specimen fabrication

Ring core specimens were fabricated to analyze the influence of the internal vertical air gap structures in soft magnetic components. The ring core specimens had an outer diameter of 35 mm and a square cross-section with an edge length of 5 mm and were fabricated horizontally to the build platform. Ring core specimens without air gaps (bulk) and ring core specimens with air gaps in meandric formation were fabricated. The air gap height was 4.5 mm and the distance between two air gap centers was 0.625 mm. Fig. 3 shows the fabricated ring core specimens and the schematic arrangement of the air gaps. The PBF-LB process and ultrafast laser ablation were alternated in each specimen layer. Exposure of the powder layer geometries in the PBF-LB process was performed over the entire specimen surface without recessing the air gaps using a bi-directional line scanning strategy with a 90° rotation of the scan vectors between successive powder layers. Between the lowering of the build platform and the powder coating of the next specimen layer, the layer-wise laser material ablation was performed in the PBF-LB solidified specimen layer to create the air gaps. Each air gap structure was processed with 760 passes per layer to achieve continuous material-separating air gaps with the machine setup and parameters used during the PBF-LB build process. The focal positions of the laser beams are on the powder bed layer surface for the PBF-LB process and on the respective PBF-LB solidified specimen layer surface for the USP laser material ablation. To avoid oxidation during the manufacturing process, Argon 5.0 with a purity of 99.999% was used as shielding gas in the powder bed process chamber, and the residual oxygen content was kept below 200 ppm at all times. Table 1 shows the parameters used to fabricate the ring core specimens (with and without air gaps).

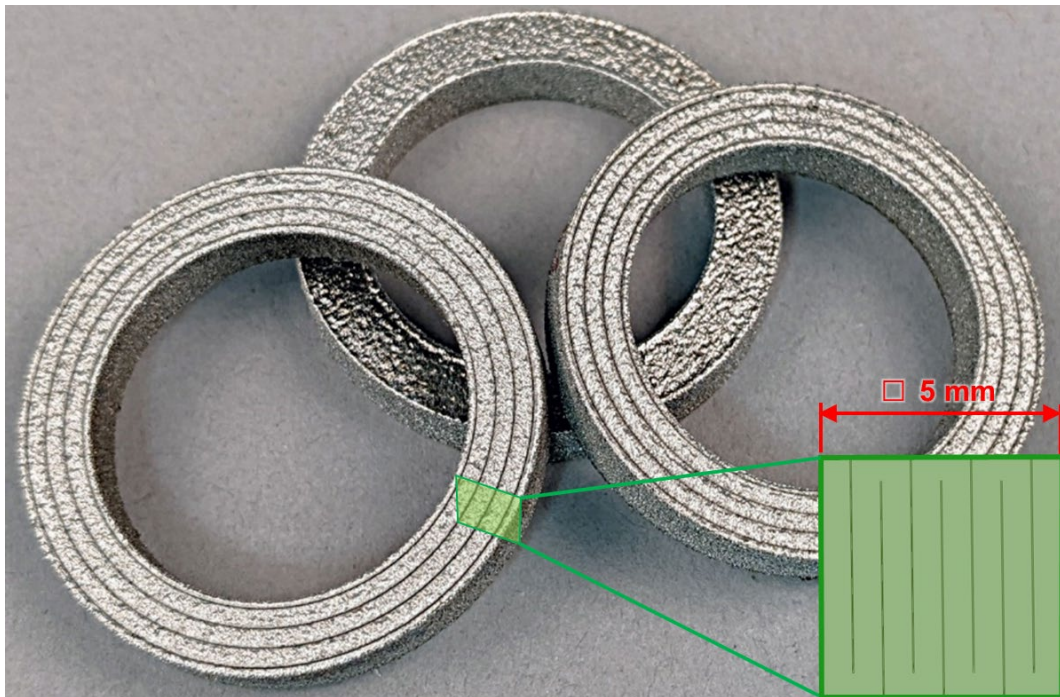


Fig. 3. Fabricated ring core specimens with air gaps (front) and bulk material without air gaps (back) together with the schematic arrangement of the air gaps

Table 1. Parameters for fabrication of the ring core specimens with and without air gaps

| Parameter | PBF-LB process (CW laser) | Ablation process (USP laser) |
|--|--|--------------------------------------|
| Wavelength | 1030 nm | 1030 nm |
| Average laser power | 515 W | 30 W |
| Pulse duration | - | 8 ps |
| Pulse frequency | - | 300 kHz |
| Pulse energy | - | 100 μ J |
| Focal diameter | 200 μ m | 35 μ m |
| Focal position | Powder bed layer surface | Solidified PBF-LB part layer surface |
| Scan speed | 1300 mm/s | 3000 mm/s |
| Hatch distance | 100 μ m | - |
| Powder layer thickness | 50 μ m | - |
| Powder/PBF-LB layer exposure strategy | Bi-directional line scanning with 90° rotation between powder layers | Circular |
| Number of passing each powder/PBF-LB layer | 1 | 760 |

2.4. Specimen characterization

The fabricated ring core specimens were subjected to Brockhaus MPG 200D magnetic characterization in the as-built (AS) and heat-treated (HT) conditions. For this purpose, the ring core specimens were separated from the build platform and the upper and lower surfaces of the specimens (with respect to the build direction) were metallographically plane-polished prior to magnetic characterization and heat treatment. Heat treatment was performed at 1150 °C for 6 h in a forming gas atmosphere (Ar + 5% H₂). The magnetic properties are calculated based on a measured fill factor, which takes into account the influence of the removed air gap volume and the porosity of the specimens. Also, the actual specimen heights were considered in the magnetic characterization.

3. Results and Discussion

3.1. Geometric properties

The density and the achieved air gap geometry of the fabricated specimens were analyzed by computed tomography (CT) of a ring core segment. The built-up part by the PBF-LB process exhibits a high density with only occasionally pores, see Fig. 4. The air gaps created by layer-wise ultrafast laser ablation are uniform and exhibit only very isolated contact points due to the precise surface structures. The width of the air gaps is mostly in the range of 25-45 μ m, see Fig. 4 b).

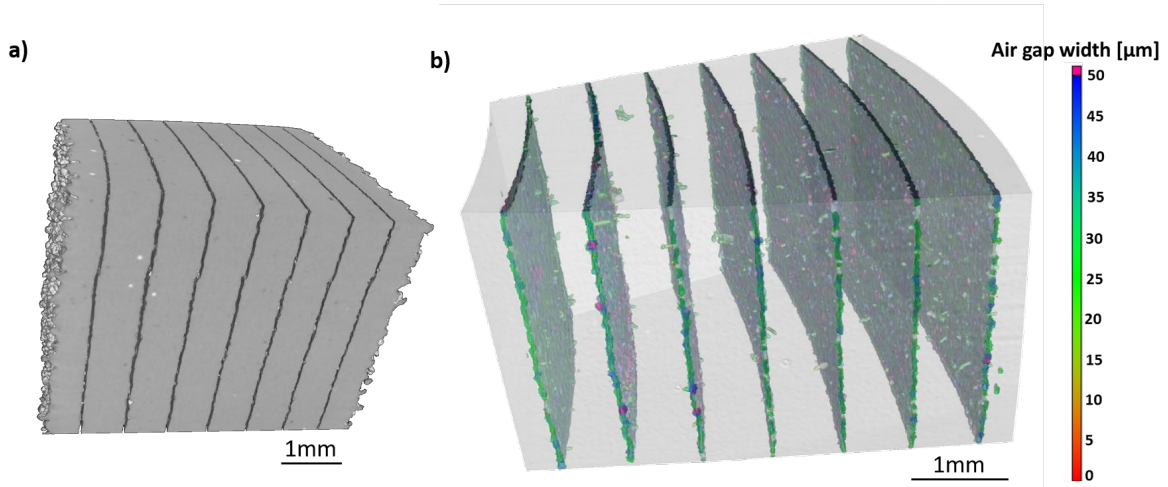


Fig. 4. (a) CT scan of a segment of the ring core specimen with air gaps; (b) Visualization of the variation in air gap width

3.2. Magnetic performance

At the as-built state, the bulk ring core specimen and the specimen with integrated air gaps exhibits a similar coercivity of 320 A/m to 343 A/m, see Fig. 5 a). With increasing magnetic field strength H , the integrated air gaps cause a faster flattening of the resulting magnetic flux density J curve. After heat treatment, the coercivity is greatly reduced to 78 A/m for the bulk specimen and 30 A/m for the ring core with integrated air gaps. Thus, the heat treatment can greatly minimize the hysteresis losses. Afterwards, only slight differences between the specimen geometries can be detected (see Fig. 5 b)).

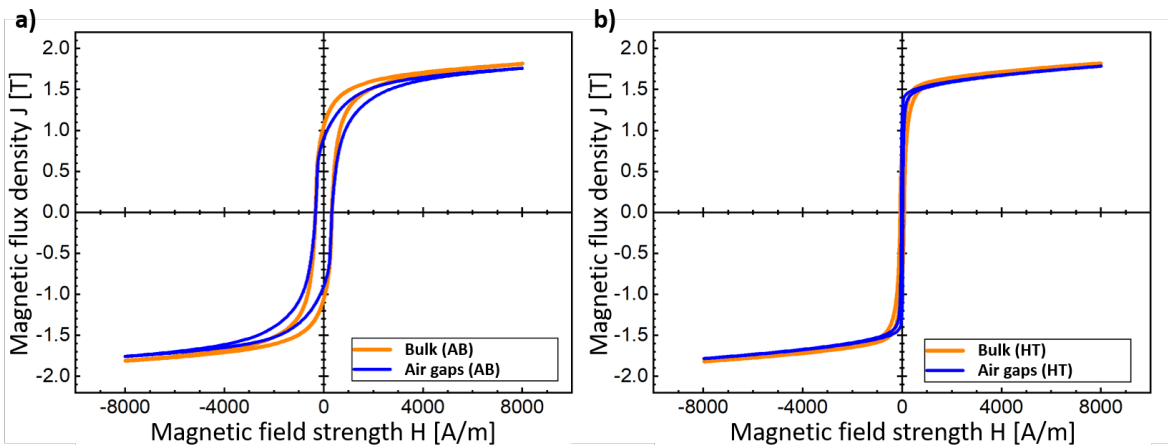


Fig. 5. Room temperature DC hysteresis loop of the ring core specimen with air gaps compared to the bulk ring core specimen. The maximum applied magnetic field is 8000 A/m, i.e., the saturation magnetization value is not reached during the JH-curve measurement. (a) Hysteresis curve in the as-built (AB) condition; (b) Hysteresis curve in the heat-treated (HT) condition

Fig. 6 shows the measured iron losses P_s of the fabricated ring core specimens in the as-built condition and in the heat-treated condition without air gaps (bulk) and with air gaps as a function of the remagnetization frequency f ranges from 25 to 200 Hz at a peak polarization of a) 0.1 T and b) 0.2 T, respectively. The iron losses, excited at 0.1 T, increase for the bulk specimen in the as-built condition from 194 W/kg at a frequency of 25 Hz to 3338 W/kg at a frequency of 200 Hz. In the heat-treated condition, this is 68% lower at 1080 W/kg at $f = 200$ Hz. The introduction of circumferential air gap geometries at a remagnetization frequency f of 200 Hz achieves a reduction in iron losses of about 40% to 1993 W/kg in the as-built condition and a reduction of about 22% to 846 W/kg in the heat-treated condition. Comparable improvements were obtained at a higher peak polarization of 0.2 T (see also Table 2). The reduction in iron losses is due to the introduction of the air gaps and the associated spatially reduced eddy currents. Compared to the as-built condition, this effect is less pronounced in the heat-treated condition.

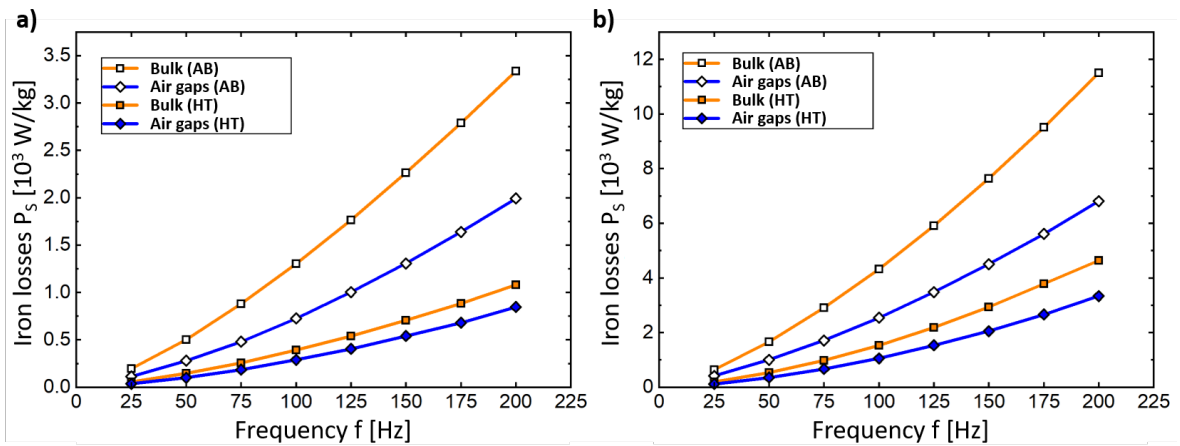


Fig. 6. Iron losses P_s in as-built (AB) and heat-treated (HT) condition of the ring core specimen with air gaps compared to the bulk ring core specimen. For the measurements, the frequency f of the alternating field has been varied between 25 and 200 Hz. (a) Peak polarization 0.1 T; (b) Peak polarization 0.2 T

Table 2. Iron losses P_s and percentage improvement due to subtractive air gaps as a function of remagnetization frequency f , specimen condition and air gap geometry, measured with a peak polarization of 0.1 T and 0.2 T

| Frequency f | Iron losses P_s [10^3 W/kg] | | | | | |
|----------------|----------------------------------|----------|--------------|----------|-------------------------|--------------|
| | As-Built | | Heat-Treated | | Enhancement by air gaps | |
| | Bulk | Air gaps | Bulk | Air gaps | As-Built | Heat-Treated |
| 25 Hz @ 0.1 T | 194 | 113 | 57 | 36 | 41.8% | 36.8% |
| 100 Hz @ 0.1 T | 1302 | 726 | 392 | 289 | 44.2% | 26.3% |
| 200 Hz @ 0.1 T | 3338 | 1993 | 1080 | 846 | 40.3% | 21.7% |
| 25 Hz @ 0.2 T | 645 | 415 | 197 | 120 | 35.7% | 39.1% |
| 100 Hz @ 0.2 T | 4324 | 2545 | 1527 | 1057 | 41.1% | 30.8% |
| 200 Hz @ 0.2 T | 11498 | 6806 | 4632 | 3334 | 40.8% | 28.0% |

4. Conclusion and Outlook

In this research work, the use of a quasi-simultaneous additive and subtractive laser manufacturing process to enhance additively manufactured soft magnetic components by creating precise vertical narrow air gaps is investigated. By combining the PBF-LB process with layer-wise ultrafast laser ablation, a precise air gap width of approximately 25–45 μm was achieved inside the pure iron soft magnetic components, which significantly exceeds the geometric limits of pure PBF-LB. As a result, the soft magnetic properties in the alternating magnetic field at frequencies of 25–200 Hz investigated here could be improved by up to 44% in the as-built state and by up to 39% in the heat-treated state by integrating the air gaps with layer-wise ultrafast laser ablation compared to the PBF-LB bulk specimen.

The ongoing research focuses on the processing of higher-performance soft magnetic materials, such as high silicon content iron materials. For processing such PBF-LB thermally crack-sensitive materials, a build platform heating system is currently being integrated into the modular powder bed system. In addition, the fabrication of internal complex 3D air freeform geometries by using the combined additive-subtractive laser manufacturing process is currently being investigated. Future work will also investigate magnetic characterization at higher remagnetization frequencies and peak polarizations as these directly affect iron losses and thus the soft magnet performance.

Acknowledgements

The authors acknowledge support by the Ministry of Science, Research and the Arts of the Federal State of Baden-Württemberg for the financial support of the ADDSUB and FutureM projects within the InnovationCampus Future Mobility (ICM). We would also like to thank Dr. Thomas Kresse of the Materials Research Institute (IMFAA) at Aalen University for the characterization of the magnetic properties and Torsten Kunert (IMFAA) as well as Florian Mäuser from Gießerei Technologie Aalen (GTA) at Aalen University for the computed tomography analyses.

References

- Lamichhane, T. N., Sethuraman, L., Dalagan, A., Wang, H., Keller, J., & Paranthaman, M. P., 2020. Additive manufacturing of soft magnets for electrical machines—a review, *Materials Today Physics* 15, 100255.
- Pham, T., Kwon, P., & Foster, S., 2021. Additive Manufacturing and Topology Optimization of Magnetic Materials for Electrical Machines—A Review, *Energies* 14, 283.
- Giannotta, N., Sala, G., Bianchini, C., & Torreggiani, A., 2023. A Review of Additive Manufacturing of Soft Magnetic Materials in Electrical Machines, *Machines* 11, 702.
- Garibaldi, M., Ashcroft, I., Lemke, J. N., Simonelli, M., & Hague, R., 2018. Effect of annealing on the microstructure and magnetic properties of soft magnetic Fe-Si produced via laser additive manufacturing, *Scripta Materialia* 142, p. 121–125.
- Plotkowski, A., Pries, J., List, F., Nandwana, P., Stump, B., Carver, K., & Dehoff, R. R., 2019. Influence of scan pattern and geometry on the microstructure and soft-magnetic performance of additively manufactured Fe-Si, *Additive Manufacturing* 29, 100781.
- Goll, D., Schuller, D., Martinek, G., Kunert, T., Schurr, J., Sinz, C., Schubert, T., Bernthaler, T., Riegel, H., & Schneider, G., 2019. Additive manufacturing of soft magnetic materials and components, *Additive Manufacturing* 27, p. 428–439.
- Tiismus, H., Kallaste, A., Belahcen, A., Tarraste, M., Vaimann, T., Rassõlkin, A., Asad, B., & Shams Ghahfarokhi, P., 2021. AC Magnetic Loss Reduction of SLM Processed Fe-Si for Additive Manufacturing of Electrical Machines, *Energies* 14, 1241.
- Kresse, T., Schurr, J., Lanz, M., Kunert, T., Schmid, M., Parspour, N., Schneider, G., & Goll, D., 2022. Additively Manufactured Transverse Flux Machine Components with Integrated Slits for Loss Reduction, *Metals* 12, 1875.
- Goodall, A. D., Yiannakou, G., Chechik, L., Mitchell, R. L., Jewell, G. W., & Todd, I., 2023. Geometrical control of eddy currents in additively manufactured Fe-Si, *Materials & Design* 230, 112002.

- Henn, M., Buser, M., Onuseit, V., Weber, R., & Graf, T., 2021. Combining LPBF and ultrafast laser processing to produce parts with deep microstructures, Laser in Manufacturing Conference 2021, Proceeding.
- Henn, M., Buser, M., Onuseit, V., Weber, R., & Graf, T., 2022. Increasing the precision of Laser-Based Powder Bed Fusion by process combination with in situ laser ablation, Procedia CIRP 111, p. 61–64.